

REPORT DOCUMENTATION PAGE			Form Approved OMB No. 0704-0188		
Public reporting burden for this collection of information is estimated to average 1 hour per response, including the time for reviewing instructions, searching existing data sources, gathering and maintaining the data needed, and completing and reviewing this collection of information. Send comments regarding this burden estimate or any other aspect of this collection of information, including suggestions for reducing this burden to Department of Defense, Washington Headquarters Services, Directorate for Information Operations and Reports (0704-0188), 1215 Jefferson Davis Highway, Suite 1204, Arlington, VA 22202-4302. Respondents should be aware that notwithstanding any other provision of law, no person shall be subject to any penalty for failing to comply with a collection of information if it does not display a currently valid OMB control number. PLEASE DO NOT RETURN YOUR FORM TO THE ABOVE ADDRESS.					
1. REPORT DATE (DD-MM-YYYY) 13-12-2005		2. REPORT TYPE Technical Paper		3. DATES COVERED (From - To)	
4. TITLE AND SUBTITLE O+HCl Chemistry Models for Hypervelocity Collisions in DSMC				5a. CONTRACT NUMBER	
				5b. GRANT NUMBER	
				5c. PROGRAM ELEMENT NUMBER	
6. AUTHOR(S) T. Ozawa and D.A. Levin (Penn State Univ.); I.J. Wysong (AFRL/PRSA)				5d. PROJECT NUMBER 2308	
				5e. TASK NUMBER 0532	
				5f. WORK UNIT NUMBER	
7. PERFORMING ORGANIZATION NAME(S) AND ADDRESS(ES) Air Force Research Laboratory (AFMC) AFRL/PRSA 10 E. Saturn Blvd. Edwards AFB CA 93524-7680				8. PERFORMING ORGANIZATION REPORT NUMBER AFRL-PR-ED-TP-2005-486	
9. SPONSORING / MONITORING AGENCY NAME(S) AND ADDRESS(ES) Air Force Research Laboratory (AFMC) AFRL/PRS 5 Pollux Drive Edwards AFB CA 93524-7048				10. SPONSOR/MONITOR'S ACRONYM(S)	
				11. SPONSOR/MONITOR'S NUMBER(S) AFRL-PR-ED-TP-2005-486	
12. DISTRIBUTION / AVAILABILITY STATEMENT Approved for public release; distribution unlimited. PA number AFRL-ERS-PAS-05-308.					
13. SUPPLEMENTARY NOTES Presented at the 44 th AIAA Aerospace Sciences Meeting and Exhibit, 9-12 Jan 2006, Reno, NV. AIAA Paper 2006-1193.					
14. ABSTRACT In earlier work, atmospheric-jet interaction flows were simulated using direct simulation Monte Carlo (DSMC) calculations for altitudes of 80, 120 and 160 km. At high altitudes, the $O(^3P)+HCl(^1\Sigma^+) \rightarrow OH(^2\Pi)+Cl(^2P)$ reaction was found to contribute the most to OH production. However, the total collision energy (TCE) reaction probability was often found to be unphysically greater than unity. In this work, we examine in detail different reaction models such as the TCE model using the rate constants of Mahmud <i>et al.</i> and Xie <i>et al.</i> In addition to the TCE model, quasi-classical trajectory (QCT) calculations were performed to obtain the reaction probability for the O+HCl reaction with the new benchmark triplet A'' and A' surfaces. Both reaction and total collision cross sections were calculated by the QCT method. The dynamic molecule collision model was used to calculate the viscosity cross section from which the VHS-equivalent collision cross sections were derived. The tabulated QCT reaction probabilities were then used in the DSMC calculations to model OH production at 120 km. It is found that the QCT-based collision cross sections are greater than the Bird VHS cross sections, and the QCT reaction probabilities for O+HCl are lower than the TCE probabilities using the rate of Mahmud <i>et al.</i> Using the QCT reaction probability, the maximum reaction probability for the O+HCl reaction was found to be lower than 0.4 in the atmospheric-jet interaction flows for an altitude of 120 km and a freestream velocity of 5 km/s.					
15. SUBJECT TERMS					
16. SECURITY CLASSIFICATION OF:			17. LIMITATION OF ABSTRACT A	18. NUMBER OF PAGES 19	19a. NAME OF RESPONSIBLE PERSON Dr. Ingrid J. Wysong
a. REPORT	b. ABSTRACT	c. THIS PAGE			19b. TELEPHONE NUMBER (include area code)
Unclassified	Unclassified	Unclassified			(661) 275-5206

O+HCl Chemistry Models for Hypervelocity Collisions in DSMC

T. Ozawa* and D. A. Levin†

The Pennsylvania State University, University Park, PA 16802-144

and

I. J. Wysong‡

Edwards Air Force Base, AFRL-PRSA, Edwards AFB, CA 93524

In earlier work,¹ atmospheric-jet interaction flows were simulated using direct simulation Monte Carlo (DSMC) calculations for altitudes of 80, 120 and 160 km. At high altitudes, the $O(^3P)+HCl(^1\Sigma^+) \rightarrow OH(^2\Pi)+Cl(^2P)$ reaction was found to contribute the most to OH production. However, the total collision energy (TCE) reaction probability was often found to be unphysically greater than unity. In this work, we examine in detail different reaction models such as the TCE model using the rate constants of Mahmud *et al.*² and Xie *et al.*³ In addition to the TCE model, quasi-classical trajectory (QCT) calculations were performed to obtain the reaction probability for the O+HCl reaction with the new benchmark triplet A'' and A' surfaces.⁴ Both reaction and total collision cross sections were calculated by the QCT method. The dynamic molecule collision model was used to calculate the viscosity cross section from which the VHS-equivalent collision cross sections were derived. The tabulated QCT reaction probabilities were then used in the DSMC calculations to model OH production at 120 km. It is found that the QCT-based collision cross sections are greater than the Bird VHS cross sections, and the QCT reaction probabilities for O+HCl are lower than the TCE probabilities using the rate of Mahmud *et al.* Using the QCT reaction probability, the maximum reaction probability for the O+HCl reaction was found to be lower than 0.4 in the atmospheric - jet interaction flows for an altitude of 120 km and a freestream velocity of 5 km/s.

Nomenclature

χ	Deflection angle
η	Viscosity coefficient
\hat{e}'_{int}	Dimensionless post-collisional internal energy
\hat{e}_{int}	Dimensionless internal energy
\hat{e}_{tr}	Dimensionless translational energy
\hat{g}	Dimensionless relative velocity

*Graduate Research Assistant, Department of Aerospace Engineering, 135 Hammond Building, University Park, PA 16802. Student Member AIAA.

†Associate Professor, Department of Aerospace Engineering; dalevin@psu.edu. 233 Hammond Building, University Park, PA 16802. Associate Fellow AIAA.

‡Ingrid.Wysong@edwards.af.mil. 10 E Saturn Blvd, Edwards AFB, CA, 93524. Associate Fellow AIAA.

Copyright © 2006 by the American Institute of Aeronautics and Astronautics, Inc. The U.S. Government has a royalty-free license to exercise all rights under the copyright claimed herein for Governmental purposes. All other rights are reserved by the copyright owner.

\hat{g}'	Dimensionless post-collisional relative velocity
μ	Reduced mass
ν	Coefficient of viscosity
ω	Viscosity index ($\omega = \nu - 0.5$)
ϕ	Initial direction of rotational vector
ψ	Initial orientation of molecules
σ_r	Reaction cross section
σ_T	Total collision cross section
σ_μ	Viscosity cross section
σ_{el}	Elastic collision cross section
σ_{tr}	Inelastic collision cross section
σ_T^{VHS}	VHS collision cross section
ζ_v	Effective number of degrees of freedom for vibration
b	Impact parameter
d	Diameter
E_c	Collision energy
E_a	Activation energy
E_{int}	Internal energy
E_{tr}	Translational energy
g	Relative velocity
J	Rotational quantum number
k	Boltzmann constant
K_f	Reaction rate constant
m	Mass of a molecule
P_r	Reaction probability
Q_{int}	Partition function for internal modes
Q_{rot}	Rotational partition function
Q_{vib}	Vibrational partition function
v	Vibrational quantum number

I. Introduction

The modeling and simulation of chemically reacting flows caused by the interaction of a jet positioned on the side of a hypersonic rocket is a challenging. The forward and aft reaction control systems (RCS) engines provide the thrust for attitude maneuvers to control the vehicle trajectory. The investigation of the interaction of RCS jets with the rarefied atmosphere is needed at high altitudes since the relative velocities of the freestream atomic oxygen-plume chemical species are sufficiently high to produce chemical species that can radiate in various portions of the optical spectrum. We consider a generic RCS-vehicle geometry with freestream conditions corresponding to those of high altitude, hypersonic flight for a lateral side jet thrusting perpendicular to the rocket velocity vector into a near-vacuum environment. An important feature of the jet interaction are the hypervelocity chemical reactions between the jet and atmospheric species that occur for reactant conditions very far from the conditions for which the Arrhenius kinetic rates were obtained.

In earlier work,¹ we demonstrated the utility of direct simulation Monte Carlo (DSMC)⁵ simulations at 80, 120, and 160 km altitudes. The entire set of the chemical reactions between thruster side jet and plume-atmospheric species includes reactions between oxygen and nitrogen species as well as ones that either produce or consume OH (see Table 1). The complete list of chemical reactions modelled in the DSMC simulations may be found in Ref. 1. The first three reactions in Table 1 involve the dissociation of water by freestream constituents, N_2 , O_2 , and O . The relative importance of these three reactions will change with altitude. The last four reactions are exchange reactions between the freestream and plume constituents. The following two exchange reactions, $O+H_2$ and $O+HCl$, are potentially important because both H_2 and HCl

are present in relatively large mole fractions of divert solid propellant motors. At altitudes of 120 km and higher, O exchange with HCl was found to contribute more than 70 % of the OH produced.¹ Also, it was not possible to establish a consistent trend in terms of the relative contributions of the OH producing chemical reactions as a function of altitude.

A detailed study of the DSMC flowfield calculation at 120 km altitude for a freestream velocity of 5 km/s illustrated an important problem in the reaction model for O+HCl. A schematic of the flow geometry for the RCS jet plume-atmospheric interaction is given in Fig. 1. Figure 2 shows the spatial distribution of the total collision energy (TCE)⁶ reaction probability for O+HCl \rightarrow OH+Cl in the X-Y plane. The interaction region ahead of the jet is seen for an altitude of 120 km and a freestream velocity of 5 km/s. It is observed that the TCE reaction probabilities for this reaction are greater than one in the interaction region. Figure 3 shows the distribution of the TCE reaction probability for all of the O+HCl \rightarrow OH+Cl reactions, with the result that more than 10 percent of the reactions have a probability greater than one. Since the reaction probability cannot be greater than one, the specific implementation used in Ref. 1 was to artificially limit the reaction in all cases. This essentially causes a much smaller number of reactions to occur in the simulation compared to that governed by the Arrhenius equation.

For hypervelocity collisions, such as occur in the atmospheric - jet interaction flows, the extension of the reaction rate for the O+HCl reaction to temperatures higher than 3,000 K and the subsequent use of the rate in the TCE model are problematic. In order to reevaluate the adequacy of the present model for the O+HCl reaction, it was decided to improve upon the TCE model by use of a more exact, fundamental approach that uses the molecular dynamics/quasi-classical trajectory (MD/QCT) method to calculate the reaction collision cross sections. In addition, the Dynamic Molecular Collision (DMC) model was used to calculate both total collision cross sections and viscosity collision cross sections, and the MD/QCT viscosity collision cross sections were compared with those of the variable hard sphere (VHS) model.

Table 1. Freestream-plume species reactions for OH production reactions used in the TCE model

Reaction	$A, \text{ m}^3/\text{s}$	n	$E_a, \times 10^{-19} \text{ J}$
$\text{H}_2\text{O} + \text{N}_2 \rightarrow \text{OH} + \text{H} + \text{N}_2$	5.81×10^{-15}	0.00	7.314
$\text{H}_2\text{O} + \text{O}_2 \rightarrow \text{OH} + \text{H} + \text{O}_2$	1.13×10^{-7}	-1.31	8.197
$\text{H}_2\text{O} + \text{O} \rightarrow \text{OH} + \text{H} + \text{O}$	1.13×10^{-7}	-1.31	8.197
$\text{H}_2\text{O} + \text{O} \rightarrow \text{OH} + \text{OH}$	1.13×10^{-16}	0.00	1.275
$\text{H} + \text{O}_2 \rightarrow \text{OH} + \text{O}$	1.66×10^{-16}	0.00	1.061
$\text{O} + \text{H}_2 \rightarrow \text{OH} + \text{H}$	3.12×10^{-16}	0.00	0.952
$\text{OH} + \text{Cl} \rightarrow \text{O} + \text{HCl}$	3.10×10^{-27}	2.91	0.070
$\text{O} + \text{HCl} \rightarrow \text{OH} + \text{Cl}$ (Mahmud) ²	5.60×10^{-27}	2.87	0.244
$\text{O} + \text{HCl} \rightarrow \text{OH} + \text{Cl}$ (Xie) ³	1.70×10^{-22}	1.485	0.408

The MD/QCT modeling builds on the work of Ozawa *et al*⁷ wherein the TCE chemical reaction model⁶ was compared with MD/QCT calculations for reactions related to the production of OH in a bow-shock. The MD/QCT method enables the physical investigation into reaction cross sections, viscosity cross sections as well as total collision cross sections. It was found that at higher altitudes, the discrepancy between the TCE and MD model was larger due to the greater thermal non-equilibrium. The MD/QCT model is less affected by the translational energy, compared to the TCE model, but it is more sensitive to the reactant internal energy.

The outline of the remainder of this paper is as follows. The MD/QCT modeling of the reaction and

total cross sections is presented in Sec. II and compared with the results of the TCE model using newer Arrhenius parameters as well as more accurate O+HCl viscosity values at high temperatures. In Sec. III, we discuss the specific DSMC numerical parameters used for the single freestream condition that we examine here, 120 km, 5 km/s. Finally, in Sec. IV, we present detailed comparisons of the MD/QCT results with the TCE model and compare the changes observed in the DSMC simulation for the different chemical reaction parameters for the O+HCl reaction. Although there are multiple chemical reactions that contribute to the production of OH, we limit our discussion to the O+HCl reaction since this is the most energetically favorable reaction path.

II. MD/QCT Modeling of the Reaction Probability and Total Cross Section

A. MD/QCT Reaction Probability

The widely used method for calculating the reaction probabilities in DSMC is the TCE model.^{5,6} In this model, the reaction probability has a special form that allows one to match experimental reaction rates $K_f(T)$ in modified Arrhenius form,

$$K_f = AT^n \exp(-E_a/kT), \quad (1)$$

where A is the preexponential factor, n is the temperature dependence, and E_a is the activation energy. The Arrhenius data presented in the Table 1 were used to calculate the reaction cross sections based on the TCE model. In our previous work,¹ the rate of Mahmud *et al.*,² $A = 5.6 \times 10^{-27}$ m³/molec/s, $n = 2.87$, and $E_a = 2.44 \times 10^{-20}$ J, was used for O+HCl→OH+Cl, but in this work, a newer Arrhenius expression based on the calculations of Xie *et al.*³ was used.

A parallel MD code was developed to calculate the reaction and viscosity cross sections using the QCT-internal energy quantum mechanical threshold (QCT-IEQMT) method.⁸ For the O+HCl→OH+Cl, the *ab initio*³ A'' potential energy surface of Ramachandran and Peterson (RP)⁴ was utilized. This surface was also utilized by Xie *et al.*, who computed both QM and QCT reaction cross sections for a range of energies.⁹ The present results agree closely with those of Xie's for the same energy conditions. However, it was necessary for us to perform our own MD/QCT calculations since a large set of probabilities are required for the DSMC flowfield simulation, and we require cross sections for total collision energy values of E_c up to 8×10^{-19} J. In addition, DSMC uses continuum vibrational and rotational energies, requiring a table of probabilities for a range of E_{int} , while Xie *et al.* computed reaction cross sections for $v=0,1$, and 2 states only.

The MD/QCT reaction probability is the ratio of the reaction cross section obtained by the QCT-IEQMT method to the total collision cross section. An efficient Monte Carlo numerical procedure is utilized to evaluate the multidimensional integrals associated with averaging of the scattering geometric properties before a collision. The Monte Carlo method converges at a rate that is independent of the dimensionality of the integral. In order to utilize the Monte Carlo method, the specific initial states of each of the trajectories that correspond to the desired reaction cross section, such as $\sigma(T)$, $\sigma(v, j, E_{tr})$ or $\sigma(E_{int}, E_{tr})$ are needed. Microcanonical sampling enables one to efficiently sample the initial states of the target molecule of equal energy to obtain the trajectory initial conditions necessary to perform the MD/QCT calculations.¹⁰ For the DSMC simulations, the reaction probability of a chemical reaction as a function of translational energy E_{tr} and molecular internal energy E_{int} , is used. The reaction cross section is obtained by evaluating whether a O+HCl collision ends in a chemical reaction by

$$\sigma_r = \pi b_{max}^2 \frac{N_r}{N_T} \quad (2)$$

where N_r is the number of trajectories that result in a reaction and N_T is the number of total trajectories. In previous work,⁷ the reaction probability was assumed to be

$$P_r = \frac{\sigma_r}{\sigma_{VHS}} \quad (3)$$

where the collision cross section was found to be very close to the VHS cross section using Bird values.⁵ For the O+HCl case, however, it will be shown that the MD/QCT total cross section is different than that given by the VHS model and a different relationship will be used to obtain the MD/QCT reaction probability.

B. Total Collision Cross Section

As mentioned above, in our previous work, the variable hard sphere (VHS) model with Bird values was used for the total collision cross section. The VHS cross section is defined by $\sigma_T^{VHS} = \pi d^2$ with⁶

$$d = d_{ref}[2kT_{ref}/(\mu g^2)^\omega / \Gamma(2 - \omega)]^{1/2}, \quad (4)$$

where $\omega = 0.375$, $d_{ref} = 4.38$ Å, and $T_{ref} = 273$ K for the O+HCl reaction in Ref. 5. The reference diameters are calculated from the viscosity data,

$$d_{ref} = \left(\frac{30(mkT_{ref}/\pi)^{1/2}}{4(5 - 2\omega)(7 - 2\omega)\mu_{ref}} \right)^{1/2}. \quad (5)$$

One could also attempt to calculate the total collision cross section for the RP potential surface, but the unbounded nature of a classical total cross section for a realistic potential comes into play. To illustrate, one may use the MD/QCT method to compute,

$$\sigma_T = \pi b_{max}^2 \frac{N_c}{N_T} \quad (6)$$

where N_c is the number of trajectories that result in a collision and N_T is the number of total trajectories. However, in order to decide whether a collision has occurred, the cut-off deflection angle χ is needed, and σ_T was found to be strongly dependent on the cut-off angle χ for the O+HCl system.

Figures 4 and 5 show the distribution of the deflection angle χ for O+HCl collision at $E_{int} = 0.5 \times 10^{-19}$ and 2.0×10^{-19} J, respectively, for three different relative collision velocities obtained from our MD/QCT calculations. These HCl internal energies were chosen because these numbers are in the energy range of interest in the flowfield freestream conditions at 120 km and velocity of 5 km/s. As may be seen in the figures, the translational and internal energies increase, the peak deflection angle χ shifts to small angles. Note that the deflection angle distribution shown in Fig. 4 is based on a smaller range of impact parameters than that for Fig. 5. Our QCT procedure only considered trajectories out to the impact parameter value where the reaction probability became negligible. Thus, the higher E_{int} case considers trajectory samples from higher impact parameter values. This fact leads to the visibly lower occurrence of high deflection angles for the $E_{int} = 2 \times 10^{-19}$ J case in Fig. 5 for $v = 3$ km/s. The MD/QCT collision cross section results change with different selected cut-off angles. (The question of whether different values of internal energy should be assigned different DSMC collision cross sections has been discussed,¹¹ but will not be considered here.) Thus, for higher internal and translational energies, the cut-off angle is more important, and it is difficult to define. Therefore, the DMC method is utilized to calculate the viscosity cross section.

For implementation in DSMC, it is more consistent to obtain a transport-based collision cross section (usually viscosity) from which to convert a reaction cross section to a reaction probability, since the DSMC method already uses the VHS model viscosity-based cross section as the basis for computing the number of collisions per cell per time-step and as the basis for collision dynamics (hard-sphere isotropic scattering). In this spirit, the work of Tokumasu and Matsumoto¹² demonstrated the Dynamic Molecular Collision (DMC) model to calculate an accurate viscosity cross section for the given potential using a Monte Carlo method for integration. While the integration over the impact parameter becomes infinite for the total collision cross section, those for classical momentum and energy transfer cross sections are finite. Therefore, the viscosity cross section was calculated first, and converted to the equivalent VHS collision cross section for each collision velocity.¹²

The viscosity cross section is calculated by the Monte Carlo evaluation of an integral given by Ref. 13

$$\sigma_{\mu,MD} = \int \left(\frac{\hat{g}^4}{4} \sin^2 \chi + \frac{1}{3} (\Delta \hat{e}_{int})^2 - \frac{1}{2} (\Delta \hat{e}_{int})^2 \sin^2 \chi \right) d\tau, \quad (7)$$

where \hat{g} is defined as $\sqrt{\mu/kT}g$, \hat{e}_{int} is nondimensionalized by kT , and $\Delta \hat{e}_{int}$ is the change of the dimensionless HCl internal energy before and after a collision. The quantities χ , \hat{g} and $\Delta \hat{e}_{int}$ are obtained from the similar MD/QCT calculations for the reaction probability except the sampling of initial trajectory conditions corresponds to the geometric pre-collisional conditions specified by $\Delta \hat{e}_{int}$. The MD viscosity cross section $\sigma_{\mu,MD}$ converges when the maximum impact parameter is selected so that the effect of potential is neglected. The integral $\int()d\tau$ specifies

$$\int () d\tau = \int_0^{b_{max}} \int_0^\pi \int_0^{2\pi} \int_0^\pi () \left[\frac{d\psi}{\pi} \right] \left[\frac{d\phi}{2\pi} \right] \left[\frac{1}{2} \sin \chi d\chi \right] [2\pi b db], \quad (8)$$

where b_{max} is the cut-off impact parameter. In addition, the viscosity coefficient η is obtained by¹⁴

$$\frac{1}{\eta} = \frac{8}{5\sqrt{2\pi\mu kT}} \frac{1}{Q_{int}} \int_0^\infty dv \int_0^\infty dJ \int_0^\infty dE_{tr} \sigma_{\mu} \frac{E_{tr}}{2kT} (2J+1) \exp\left(-\frac{\mu g^2}{2kT} - \frac{E_{vJ}}{kT}\right). \quad (9)$$

The equivalent VHS collision cross section is $\sigma_T = \pi d_t^2$, and the diameter for the total collision cross section can be obtained by

$$d_t = \sqrt{\frac{6\sigma_{\mu,MD}}{\pi \hat{g}^4}}. \quad (10)$$

III. DSMC Models, Numerical Parameters, and Freestream Conditions

Figure 1 shows the flow geometry used in the modelling of the interaction of the atmosphere and the RCS jet. A small rocket is modeled as a blunted cone cylinder and a thruster positioned on the cylinder right after the cone-cylinder junction. The radius of the cylinder is 0.2 m, and the length from the head of the cone to the nozzle exit is 2 m. In this work, the angle of attack is zero. The freestream parameters at 120 km altitude are listed in Table 2. A starting surface was obtained from the axisymmetric DSMC plume core-flow DSMC simulations. The plume core-flow DSMC simulations were performed with the nonuniform nozzle exit condition.^{1,15} The density isolines of about 6×10^{21} molecules/m³ were taken for the starting surface of a 60-lbf (270-N) thruster. The starting surface is an oval shape with approximate x and y dimensions of 0.3 and 0.5 m.

Table 2. Freestream parameters

Parameter	120 km
Temperature, K	354
Number density, molec/m ³	4.73×10^{17}
O ₂ mole fraction, %	9
N ₂ mole fraction, %	73
O mole fraction, %	18

The three-dimensional DSMC calculations were implemented in the SMILE computational tool. The gas is considered a 14-species reacting mixture. Approximately 18 million molecules were simulated in

the computational domain. Separate grids were used for collisions and macroparameters adaptive to flow gradients. The total number of collision cells was approximately 5 million. The total number of time steps was about 100,000 with a time step of 2.0×10^{-7} s. Macroparameter sampling was started after 20,000 time steps, a time sufficient to reach the steady state. These parameters were chosen to minimize the statistical dependence between simulated particles, remove the grid dependence of the results, and furnish sufficient spatial resolution of the boundary layer along the rocket.

The majorant frequency scheme¹⁶ is employed for modeling the molecular collision frequency to enhance the statistical representation. For trace species, a weighting factor of approximately 0.01 was used. The VHS model was used for modeling non-reactive interactions between particles. The Borgnakke-Larsen¹⁷ (BL) model (also see Ref. 18) with temperature-dependent rotational and vibrational relaxation numbers was chosen for modeling rotation - translation and vibration - translation energy transfer. The effective degree of freedom for vibration was modeled to be temperature-dependent. The TCE model was used to calculate the chemical reaction probabilities. For the $\text{O}+\text{HCl} \rightarrow \text{OH}+\text{Cl}$ reaction, both the TCE and MD models were used. The entire set of the chemical reactions can be found in earlier work,¹ and the OH production reactions used in this work are presented in Table 1. The gas-surface interaction was modeled using a diffuse model with total energy and momentum accommodation with a rocket wall temperature of 300 K.

IV. Results and Discussion

A. Rate Constant for $\text{O}+\text{HCl} \rightarrow \text{OH}+\text{Cl}$

Although the DSMC method requires the probability of a reaction, instead of the rate constant, the latter quantity provides a consistency check for the MD/QCT calculations presented in this work. Figure 6 presents the reaction rate constant calculated using a parallel MD code between 1,000 K and 3,000 K. The reaction rate may be calculated from the reaction cross section by averaging the target molecule (HCl) over a Maxwellian equilibrium distribution,

$$\begin{aligned}
 k_f &= f(T) Q_{vib}^{-1} Q_{rot}^{-1} \left(\frac{8kT}{\pi\mu} \right)^{1/2} \left(\frac{1}{kT} \right)^2 \\
 &\times \sum_v \sum_J (2J+1) \int_0^\infty \int_0^{b_{max}} P_r(v, J, E_{tr}, b) \\
 &\times \exp(-E_{tr}/kT) 2\pi b db E_{tr} dE_{tr},
 \end{aligned} \tag{11}$$

and for $\text{O}+\text{HCl}$,

$$f(T) = \frac{3}{5 + 3 \exp(-228/T) + \exp(-326/T)}. \tag{12}$$

The factor $f(T)$ is the probability that the target molecular system is initially on one of the three electronic surfaces that allow a reaction to occur. This temperature dependent expression accounts for the spin-orbit splitting of the overall triplet reagents. The typical number of trajectories per temperature value was approximately 20,000. Figure 6 shows that the rate of Mahmud *et al*² used in our previous DSMC calculations is higher than the QCT(RP) rate obtained with the RP surface in this work and the improved canonical variational theory (ICVT) rate constant of Xie *et al*.³ The QCT (RP) rate is slightly lower than the ICVT rate because only the $^3A''$ surface was used for QCT calculations, and the $^3A'$ surface contribution increases for higher temperature. In addition, the tunneling effect, not included in the MD/QCT calculations, is more important for lower temperature.

B. Reaction Probability for O+HCl → OH+Cl

Figure 7 shows a comparison of reaction probabilities between the MD and TCE⁶ models as a function of reactant internal energy at 3 and 5 km/s relative velocities. The MD reaction probability is calculated here as the reaction cross section divided by the VHS cross section using Bird's values.⁵ The rate of Mahmud *et al*² used for our previous simulations and the rate of Xie *et al*³ are also shown in the figure. The effective number of degrees of freedom for vibration $\zeta_{v,HCl} = 1$ is used, and the VHS model with the parameters of Ref. 5 of $\omega = 0.375$, $d_{ref} = 4.38$ Å and $T_{ref} = 273$ K was used for all the three cases in this subsection. In the next subsection, the fidelity of the VHS values used will be discussed. It can be seen that the TCE probabilities computed from the rate of Mahmud *et al* are much higher than the MD/QCT or TCE model using the Arrhenius parameters derived from the rate coefficients computed by Xie *et al* for both relative velocities. This result is consistent with our previous calculations in which the probabilities for the O+HCl reaction were found to be greater than one. For the 3 km/s case, the MD/QCT model predicts slightly higher reaction probabilities than the TCE with the rate calculations of Xie *et al*.³ Nonetheless, at 5 km/s, the discrepancy becomes more significant, and the MD/QCT model predicts higher probabilities than the TCE model. The reason for this is as follows. For the TCE model the reaction probability increases uniformly as the translational energy increases. However, the MD reaction probability does not necessarily increase uniformly as the translational energy increases.

C. Collision Cross Section for O+HCl

In the previous subsection, the VHS collision cross section with $\omega = 0.375$, $d_{ref} = 4.38$ Å and $T_{ref} = 273$ K was used. In this subsection, the preferred values for VHS for O+HCl collisions is investigated. In our earlier reported results,^{1,15} the viscosity index ω of 0.25 for O and ω of 0.5 for HCl were used,^{5,19} i.e., the HCl molecule was treated in the Maxwell model. However, although the viscosity index ω of HCl is 0.5 between 20 and 99 °C, for some gases, ω decreases as temperature increases.¹⁹ Therefore, the VHS total cross sections obtained from a Maxwell molecule may not be accurate for higher temperatures.

Let us consider the selection of the two parameters of coefficient of viscosity ν and the reference diameter d_{ref} for the VHS model. The parameters used in the previous DSMC calculations were mostly obtained from viscosity data in the low temperature range.¹⁹ Figure 8 shows the variation of viscosity coefficient of HCl from 100 to 5,000 K. In the figure, the data of Svehla²⁰ and the data (Bird) in Ref. 19 are shown. Svehla estimated the viscosities using the Lennard-Jones (12-6) potentials. From the data (Bird), the coefficient of viscosity of HCl ν_{HCl} is 1.0, and with ν_{HCl} of 1.0, the coefficient of viscosity is higher than the data of Svehla. The coefficient of viscosity of HCl ν_{HCl} of 0.65 agrees well with the data of Svehla between 1,000 and 5,000 K. The VHS parameters for HCl are listed in Table 3. It is seen that the value of ω is quite different for low and high temperatures.

Table 3. VHS parameters for HCl

Data	ω	d_{ref} , Å	T_{ref} , K
Bird	0.50	5.76	273
Svehla	0.15	3.15	5,000

Using the RP ³A'' surface in the MD/QCT calculations, the quantities such as deflection angle and the change in HCl internal energy are obtained and used in Eq. (7) to calculate the viscosity cross section. The change in HCl internal energy, \hat{e}_{int} , is obtained by analyzing the momentum of the post-collisional HCl species in each trajectory. To account for the neglect of the RP ³A'' potential, the maximum impact

parameter was selected such that the rate of translational energy transfer was less than 10 %, and the MD viscosity cross section $\sigma_{\mu,MD}$ converged. The DMC method is used in this work to obtain both the O+HCl viscosity coefficients as well as the VHS-equivalent collision cross section.

The O+HCl viscosity coefficient for high temperatures was calculated by the DMC method. Figure 9 shows a comparison of the viscosity coefficients obtained from the MD/QCT results and the O and HCl data in Ref. 19 (Bird) and data of Svehla.²⁰ To compare with the MD/QCT result we take the average of the separate O and HCl viscosity coefficients. The MD/QCT results for O+HCl are believed to be the most accurate and fall above or below the data of Refs. 19 (Bird) and 20, depending on the temperature. The agreement between the MD/QCT results and the viscosities derived from the low-temperature data of Ref. 19 is good. At higher temperatures, the difference in the MD/QCT results and the viscosities derived from the coefficients of Svehla is attributed to the simpler potential model used in the latter calculations.

Figure 10 presents a comparison of the collision cross sections between the DMC(MD/QCT) and VHS models at $E_{int} = 0.5 \times 10^{-19}$ and 2.0×10^{-19} J. For the two viscosity parameters tested in the VHS model, Fig. 10 shows that the collision cross sections are greater with high temperature data of Svehla.²⁰ The VHS cross section with $\omega_{HCl} = 0.15$ and $d_{HCl,ref} = 3.15$ at 5,000 K (Svehla) is significantly larger than the VHS cross section with $\omega_{HCl} = 0.5$ and $d_{HCl,ref} = 5.76$ at 273 K (Bird) by more than 50 %. The MD/QCT results are between the VHS cross sections obtained from the data of Ref. 5 (Bird) and those of Svehla.²⁰ Therefore, if the MD/QCT VHS-equivalent collision cross section in Eq. (10) is used, lower reaction probabilities are predicted than those that would be obtained from the VHS cross sections using the data in Ref. 5 (Bird). Also, it was found that the MD/QCT VHS-equivalent cross section does not change significantly with changes of the HCl internal energy. Since the MD/QCT VHS-equivalent cross section is not dependent on the HCl internal energy, the cross sections could be fit to the simpler VHS model. The parameters, $\omega = 0.39$ and $d_{ref,1000K} = 3.9$ Å were found to give a good fit of the MD/QCT cross sections to the VHS form. The total cross sections derived from these parameters will be designated as $\sigma_{T,MD}^{VHS}$.

The inelastic collision cross section is defined for collisions that do not react but produce a change in E_{tr} as,

$$\sigma_{tr} = \int (\Delta \hat{e}_{tr})^2 d\tau, \quad (13)$$

and is related to the total collision cross section as

$$\sigma_T = \sigma_{tr} + \sigma_{el} + \sigma_r. \quad (14)$$

The quantity $\Delta \hat{e}_{tr}$ is the change of the dimensionless translational energy before and after a collision and was calculated from the MD/QCT pre and post trajectory HCl conjugate momenta for non-reactive trajectories as,

$$\Delta \hat{e}_{tr} = \frac{\hat{g}'^2}{2} + \hat{e}_{CM} - \frac{\hat{g}^2}{2} \quad (15)$$

where \hat{e}_{CM} is the dimensionless center-of-mass translational energy. Figure 11 shows the inelastic collision cross section as a function of the relative velocity. As shown in the figure, the inelastic cross section decreases as the translational energy increases. It is also found that the inelastic cross section is a function of both the translational and internal energy. However, because the change of σ_{tr} is insignificant compared to the VHS-equivalent collision cross section, $\sigma_{T,MD}^{VHS}$ does not show a strong dependence on internal energy.

Figures 12 and 13 show a comparison of the reaction probability for O+HCl \rightarrow OH+Cl calculated by using the reaction cross section divided by either the VHS model (Bird) or $\sigma_{T,MD}^{VHS}$ at 3 km/s and 5 km/s, respectively. The VHS model with $\omega = 0.39$ and $d_{ref,1000K} = 3.9$ Å was used to represent $\sigma_{T,MD}^{VHS}$ because the MD/QCT collision cross section results agree well with the VHS model with those parameters as shown in Fig. 10. Both the MD/QCT and TCE reaction probabilities using $\sigma_{T,MD}^{VHS}$ are lower than those with the VHS cross section (Bird, $\omega_{HCl} = 0.5$) because $\sigma_{T,MD}^{VHS}$ are greater than the VHS cross sections (Bird, $\omega_{HCl} = 0.5$). However, the change in the TCE model is smaller than that in the MD/QCT model.

Figure 14 presents the distributions of the $\Delta\hat{e}_{int}$ at 5 km/s for O+HCl collision for two initial internal energies. $\Delta\hat{e}_{int}$ was calculated by $\Delta\hat{e}_{int} = \hat{e}_{int}^l - \hat{e}_{int}$. Figure 14 shows that as the initial HCl internal energy increases, the $\Delta\hat{e}_{int}$ distribution spreads. In other words, the inelastic cross section increases, as the initial internal energy increases, as is generally expected based on simple models (see e.g., Ref. 21). At $E_{int} = 0.5 \times 10^{-19}$ J, energy is mostly transferred from the translational to HCl internal modes. Figure 15 shows the distributions of the $\Delta\hat{e}_{int}$ at $E_{int} = 2.0 \times 10^{-19}$ J for different collisional translational energies. At 3 km/s, the energy is transferred from the HCl internal to translational mode. However, as the initial translational energy increases, the energy shifts from the translational to internal modes. In general the results show a tendency toward energy equilibration between modes. Where $E_{tr} > E_{int}$, the E_{int} gains and where $E_{int} > E_{tr}$, the E_{tr} gains.

D. DSMC Calculations

First, the TCE model with the rate constant of Xie *et al*³ for the O+HCl \rightarrow OH+Cl reaction was utilized for the DSMC calculation at 120 km altitude for freestream velocity of 5 km/s. For the TCE model, the VHS total collision cross section for O+HCl with $\omega = 0.375$, $d_{ref} = 4.38$ Å and $T_{ref} = 273$ K was used. Figure 16 shows the N₂ number density (molecule/m³) contour for this case. Note that the change of chemical reaction models does not affect the overall flow field. The maximum N₂ number density is about 1.2×10^{18} m⁻³ between 1 and 2 m ahead of the rocket cone. Figure 17 shows the translational temperature contour with the rate constant of Xie *et al* for the O+HCl \rightarrow OH+Cl reaction at 120 km altitude for freestream velocity of 5 km/s. Similar to the total number density, the overall translational temperature profile does change with the different reaction probabilities for the O+HCl reaction. While the high number density shock region is located between $x = -2$ and -1 m, the high temperature shock region is shifted more forward than the high number density shock region. Figure 18 shows the Mach number contour at 120 km altitude for freestream velocity of 5 km/s. The high temperature shock region and low Mach number region are nearly the same.

Secondly, the DSMC calculations were implemented with three chemical reaction models at 120 km altitude for freestream velocity of 5 km/s. For the O+HCl \rightarrow OH+Cl reaction, the TCE model with the previous rate constant² (1) and the rate constant of Xie *et al*³ (2) and the MD/QCT reaction probability (3) were used. The MD/QCT reaction probability for O+HCl \rightarrow OH+Cl used in this subsection is the ratio of the MD/QCT reaction cross section to $\sigma_{T,MD}^{VHS}$, and MD/QCT reaction probabilities were tabulated to be used in DSMC. Figure 19 shows the OH number density contours with the TCE model of the rate (2) for O+HCl at 120 km altitude for freestream velocity of 5 km/s. The maximum OH number density was about 2×10^{16} m⁻³ with this chemical reaction rate. In Figs. 20 and 21, the comparison between the three chemical reaction models is shown. Figure 20 presents the OH number density distribution along the $y = 8$ m line. Figure 21 shows the OH number density distribution along the $x = -1.5$ m line. As expected, the TCE model predicts higher OH production than the MD/QCT model. With the rate (1), the OH was produced much more than the other two cases (2) and (3) because the probability for O+HCl was significantly high as shown in Fig. 2 and 7. With the rate (2), the maximum OH number density is reduced by more than 50 %, and with the MD/QCT probability, it is reduced by a factor of 4. In the shock region, the reaction probabilities changed dramatically between the rate (1) and (2) for the TCE model. With the rate (1), the reaction probabilities result in greater than one. (In the DSMC calculation, they are set to one.) Due to the jet-atmosphere interaction, high translational energies result in high reaction probabilities for the TCE model. About 10 percent of the O+HCl collisions results in the probability greater than one with the rate (1) using the TCE model as shown in Fig. 3. In contrast, with the rate of Xie *et al* (2), most of the O+HCl collisions are predicted to have the reaction probability smaller than 0.4 (see Fig. 22). The reaction probability with the MD/QCT is further lower than the other two, and more than 80 % of the reaction had the probability of lower than 0.1 as shown in Fig. 23. Using the same VHS (Bird values) collision cross section between the TCE and MD/QCT, the TCE with the rate (2) predicts higher reaction probability than the MD/QCT as shown in Fig. 7. In contrast, if both the reaction and total collision cross sections are obtained by the MD/QCT method, the MD/QCT reaction probability becomes lower than the

TCE with the rate (2). At 5km/s, the probabilities between the MD/QCT and the TCE with the rate (2) are very close, but at 3km/s or 8km/s, the TCE probabilities with the rate (2) predicts higher than those with the MD/QCT.

V. Conclusion

The chemical reacting flows with the interaction of a jet have been simulated using the DSMC method. The objective of this work was to improve the fidelity of the chemical reaction models in DSMC, and analyze the most important chemical reaction, $O(^3P)+HCl(^1\Sigma^+) \rightarrow OH(^2\Pi)+Cl(^2P)$ in the atmosphere - jet interaction flows. The MD/QCT calculations were performed for the O+HCl reaction using the *ab initio* $^3A''$ potential energy surface of Ramachandran and Peterson (RP)⁴ for both reaction and collision cross sections. The DMC model was used to calculate the viscosity cross sections, and the VHS-equivalent collision cross sections were obtained with the assumption of isotropic scattering. Finally, the MD/QCT reaction probabilities were compared with those obtained by the TCE model with two rates.

These results show that using the same VHS collision cross section, the MD/QCT reaction probability was predicted to be lower than the TCE probability with the rate of Mahmud *et al*² used in Ref. 1 (1) and higher than the TCE probability with the rate of Xie *et al*³ (2). The TCE model with the rate (1) predicted the reaction probability higher than one in the energy range of interest. In general, the TCE model provides reasonable results if it uses reasonable Arrhenius parameter values and if there is no strong favoring in the reaction among different forms of reactant energy.

The VHS cross section is very sensitive to the viscosity parameters, and there is something of uncertainty in it. Therefore, to be more accurate, the MD/QCT total collision cross sections using the DMC model were calculated for each condition. The energy transfer between the translational and internal modes was also investigated. While the translational energy transferred to the internal energy at the initial HCl internal energy of 5×10^{-20} J, the average of energy shift was almost zero at the initial HCl internal energy of 2×10^{-19} J. However, the magnitudes of the inelastic cross sections are small compared to the total cross section. The dependence on the initial internal energy is so small that the MD/QCT VHS-equivalent collision cross sections were converted to fit the VHS with $\omega = 0.39$ and $d_{ref} = 3.9$ at 1,000 K. These values were used for the MD/QCT reaction probabilities, and these probabilities were tabulated to be used in DSMC.

The DSMC simulations were performed for the atmosphere - jet interaction flows for an altitude of 120 km and a freestream velocity 5 km/s. The chemical reaction models did not affect the overall flowfield, but affected the properties of product species, OH. Although the TCE with the rate (1) resulted in the reaction probability higher than one, the TCE with the rate (2) and MD/QCT models showed the O+HCl reaction with the probability less than 0.4. Also, the OH production was slightly lower with the MD/QCT than the TCE with the rate (2).

Acknowledgments

The research performed at the Pennsylvania State University was supported by the Air Force Office of Scientific Research Grant No. F49620-02-1-0104 administered by Dr. Mitat Birkan. Special thanks is to Dr. Sergey Gimelshein for discussing the details of the calculations.

References

- ¹Gimelshein, S. F., Levin, D. A., and Alexeenko, A. A., "Modeling of the Chemically Reacting Flows from a Side Jet at High Altitudes," *Journal of Spacecraft and Rockets*, Vol. 41, No. 4, 2004, pp. 582–591.
- ²Mahmud, K., Kim, J.-S., and Fontijn, A., "A High-Temperature Photochemical Kinetics Study of the O+HCl Reaction from 350 to 1480 K," *J. Phys. Chem.*, Vol. 94, No. 7, 1990, pp. 2994–2998.
- ³Xie, T., Bowman, J. M., Peterson, K. A., and Ramachandran, B., "Quantum Calculations of the Rate Constant for the $O(^3P)+HCl$ Reaction on New *Ab Initio* $^3A''$ and $^3A'$ Surfaces," *J. Chem. Phys.*, Vol. 119, No. 18, 2003, pp. 9601–9608.

- ⁴Ramachandran, B. and Peterson, K. A., "Potential Energy Surfaces for the $^3A'$ and $^3A'$ Electronic States of the $O(^3P) + HCl$ System," *J. Chem. Phys.*, Vol. 119, No. 18, 2003, pp. 9590–9600.
- ⁵Bird, G. A., *Molecular Gas Dynamics and the Direct Simulation of Gas Flows*, chap. 2, Clarendon, Oxford, England, U.K., 1994.
- ⁶Bird, G. A., "Monte-Carlo Simulation in an Engineering Context," *Rarefied Gas Dynamics*, edited by S. Fisher, Vol. 74, AIAA, New York, 1981, pp. 239–255.
- ⁷Ozawa, T., Fedosov, D., Levin, D. A., and Gimelshein, S. F., "Quasi-Classical Trajectory Modeling of OH Production in Direct Simulation Monte Carlo," *Journal of Thermophysics and Heat Transfer*, Vol. 19, No. 4, 2005, pp. 235–244.
- ⁸Varandas, A. J. C., Brando, J., and Pastrana, M. R., "Quasiclassical Trajectory Calculations of the Thermal Rate Coefficients for the Reactions $H(D)+O_2 \rightarrow OH(D)+O$ and $O+OH(D) \rightarrow O_2+H(D)$ as a Function of Temperature," *J. Chem. Phys.*, Vol. 96, No. 7, 1992, pp. 5137–5150.
- ⁹Xie, T., Bowman, J., Duff, J. W., Braunstein, M., and Ramachandran, B., "Quantum and Quasiclassical Studies of the $O(^3P)+HCl \rightarrow OH+Cl(^2P)$ Reaction Using Benchmark Potential Surfaces," *J. Chem. Phys.*, Vol. 122, No. 1, 2005.
- ¹⁰Severin, E. S., Freasier, B. C., Hamer, N. D., Jolly, D. L., and Nordholm, S., "An Efficient Microcanonical Sampling Method," *Chemical Physics Letters*, Vol. 57, No. 1, 1978, pp. 117–120.
- ¹¹Wysong, I. J., "Molecular Collision Models for Reacting Flows: Should Molecular Diameters Which Depend on Internal Energy States be Incorporated in DSMC Simulations?" *Rarefied Gas Dynamics*, edited by R. Brun, R. Campargue, R. Gatignol, and J. C. Lengrand, Vol. 2, AIAA, Marseille, France, 1998, pp. 3–14.
- ¹²Tokumasu, T. and Matsumoto, Y., "Dynamic Molecular Collision (DMC) Model for Rarefied Gas Flow Simulations by the DSMC Method," *Physics of Fluids*, Vol. 11, No. 7, 1999, pp. 1907–1920.
- ¹³Lordi, J. A. and Mates, R. E., "Rotational Relaxation in Nonpolar Diatomic Gases," *Physics of Fluids*, Vol. 13, No. 2, 1970, pp. 291–308.
- ¹⁴Taxman, N., "Classical Theory of Transport Phenomena in Dilute Polyatomic Gases," *Physical Review*, Vol. 110, No. 6, 1958, pp. 1235–1239.
- ¹⁵Gimelshein, S. F., Alexeenko, A. A., and Levin, D. A., "Modeling of the Interaction of a Side Jet with a Rarefied Atmosphere," *Journal of Spacecraft and Rockets*, Vol. 39, No. 2, 2002, pp. 168–176.
- ¹⁶Ivanov, M. S. and Rogasinsky, S. V., "Analysis of the Numerical Techniques of the Direct Simulation Monte Carlo Method in the Rarefied Gas Dynamics," *Soviet Journal of Numerical Analysis and Mathematical Modeling*, Vol. 3, No. 6, 1988, pp. 453–465.
- ¹⁷Borgnakke, C. and Larsen, P. S., "Statistical Collision Model for Monte Carlo Simulation of Polyatomic Gas Mixture," *J. Comp. Phys.*, Vol. 18, No. 4, 1975, pp. 405–420.
- ¹⁸Boyd, I. D., "Relaxation of Discrete Rotational Energy Distributions Using a Monte Carlo Method," *Phys. Fluids A*, Vol. 5, No. 9, 1993, pp. 2278–2286.
- ¹⁹Chapman, S. and Cowling, T. G., *The Mathematical Theory of Non-Uniform Gases, Third Edition*, chap. 12, Cambridge University Press, New York, 1970.
- ²⁰Svehla, R. A., "Estimated Viscosities and Thermal Conductivities of Gases at High Temperatures," Nasa tr r-132, 1962.
- ²¹Schwartz, R. N., Slawsky, Z. I., and Herzfeld, K. F., "Calculation of Vibrational Relaxation Times in Gases," *Journal of Chemical Physics*, Vol. 20, 1952, pp. 1591–1599.

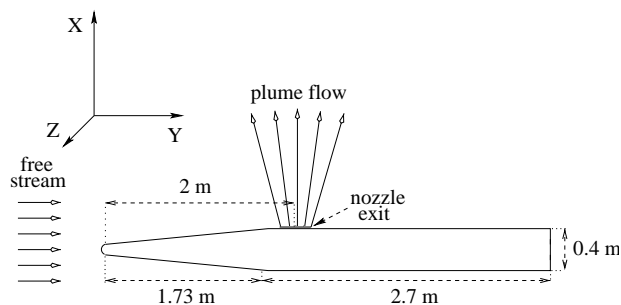


Figure 1. Schematic of the flow.

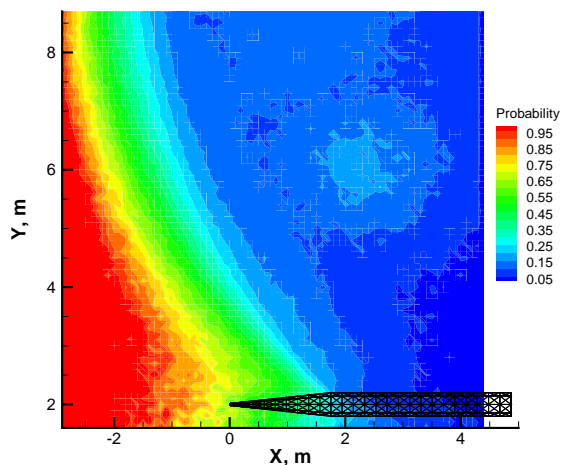


Figure 2. Reaction probability distribution in xy-plane for $O+HCl \rightarrow OH+Cl$ using the TCE model (rate constant of Mahmud *et al*²) for an altitude of 120 km and a freestream velocity 5 km/s.

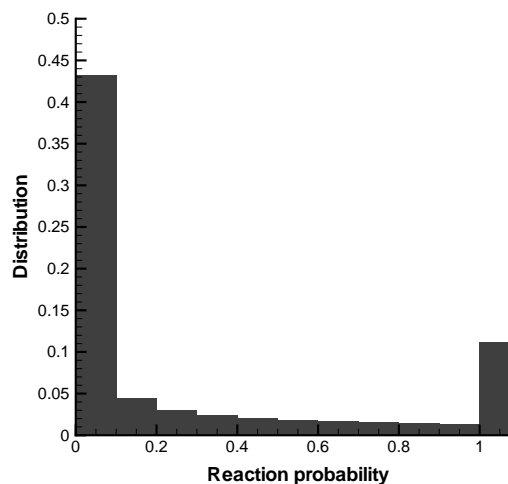


Figure 3. Reaction probability distribution for $O+HCl \rightarrow OH+Cl$ using the TCE model (rate constant of Mahmud *et al*) for an altitude of 120 km and a freestream velocity 5 km/s.

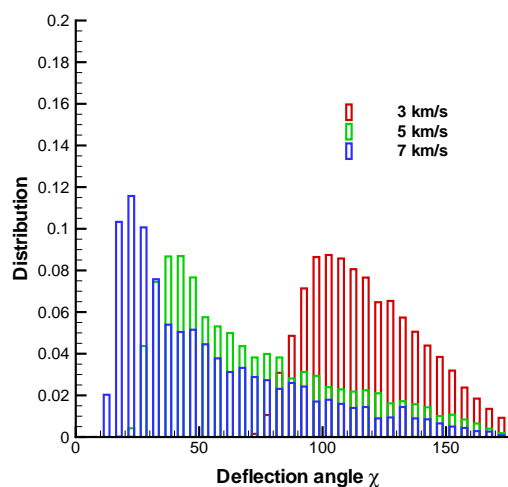


Figure 4. Distribution of the deflection angle χ for $O+HCl$ collision at $E_{int} = 0.5 \times 10^{-19}$ J: Dependence on the translational energy.

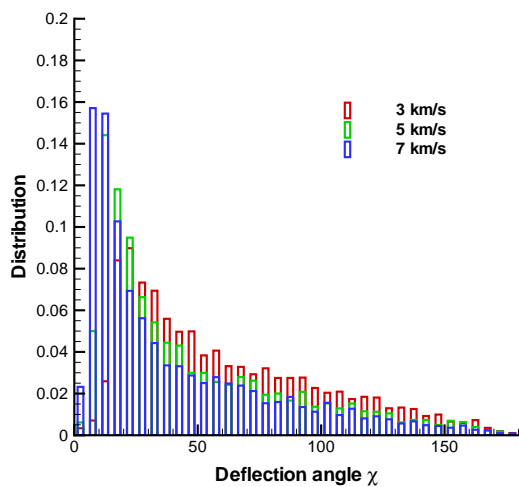


Figure 5. Distribution of the deflection angle χ for $\text{O}+\text{HCl}$ collision at $E_{int} = 2.0 \times 10^{-19}$ J: Dependence on the translational energy.

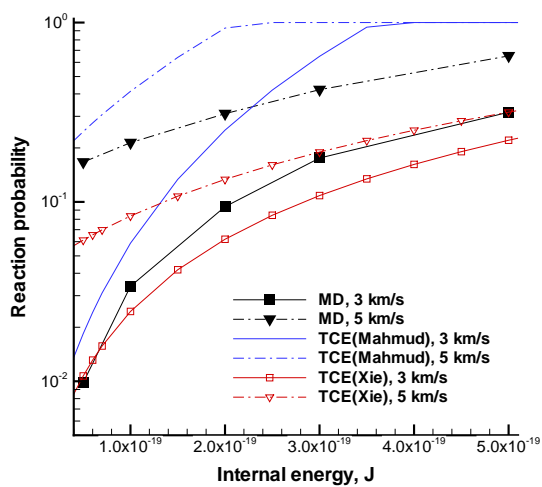


Figure 7. Comparison between MD and TCE models: Reaction probabilities for $\text{O}+\text{HCl} \rightarrow \text{OH}+\text{Cl}$ as a function of the reactant internal energy.

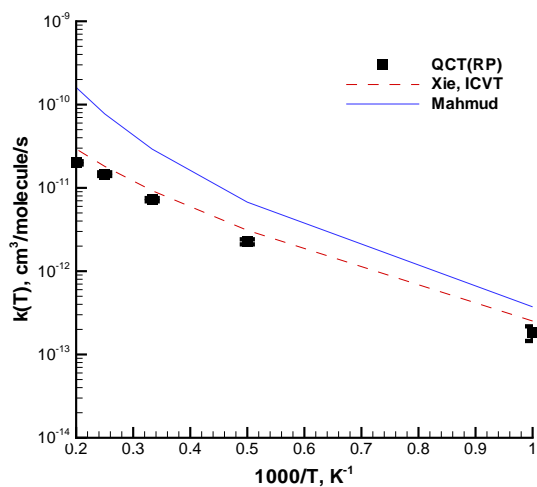


Figure 6. Reaction rate constant for $\text{O}+\text{HCl} \rightarrow \text{OH}+\text{Cl}$ as a function of temperature. The QCT(RP) is calculated in this work.

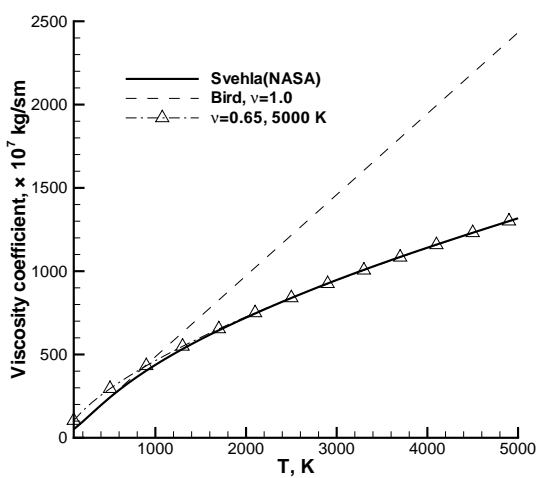


Figure 8. HCl viscosity coefficient for high temperature.

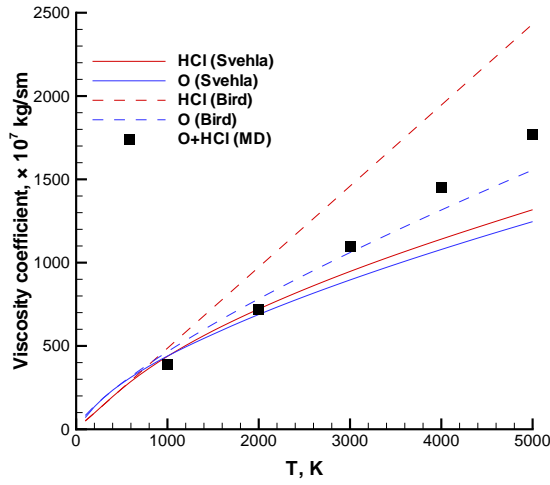


Figure 9. O+HCl viscosity for high temperatures calculated by the MD/QCT method (Eq. 9).

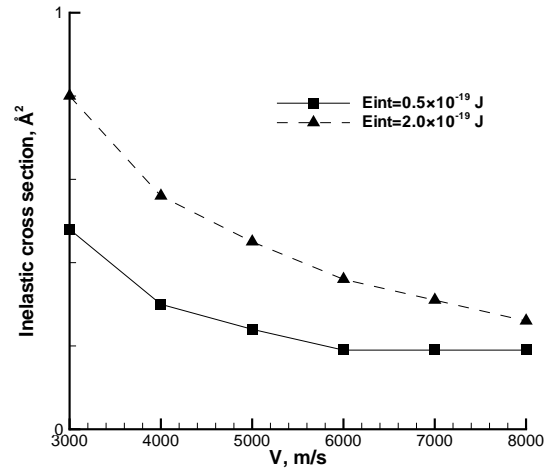


Figure 11. Comparison of inelastic collision cross sections for O+HCl collision at $E_{int} = 0.5 \times 10^{-19}$ and $E_{int} = 2.0 \times 10^{-19}$ J.

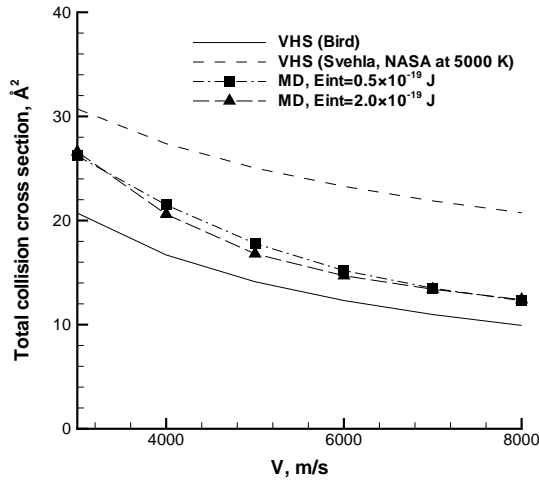


Figure 10. Comparison of total collision cross sections between MD/QCT and VHS models for O+HCl collision.

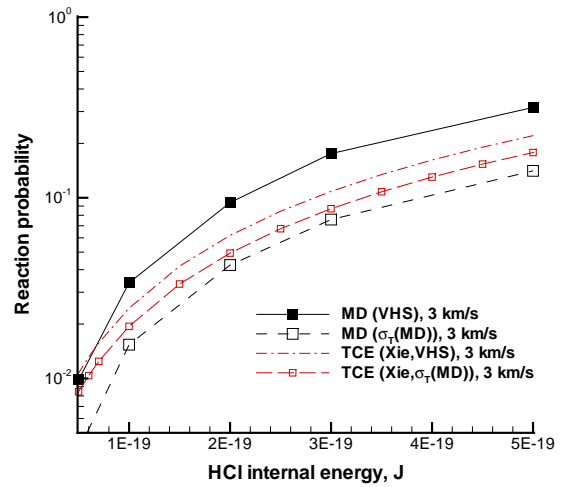


Figure 12. Comparison of the reaction probability calculated by using the reaction cross section divided by either the VHS model (Bird) or the MD/QCT total collision cross section ($\sigma_T(\text{MD})$): Reaction probabilities as a function of the reactant internal energy at 3 km/s.

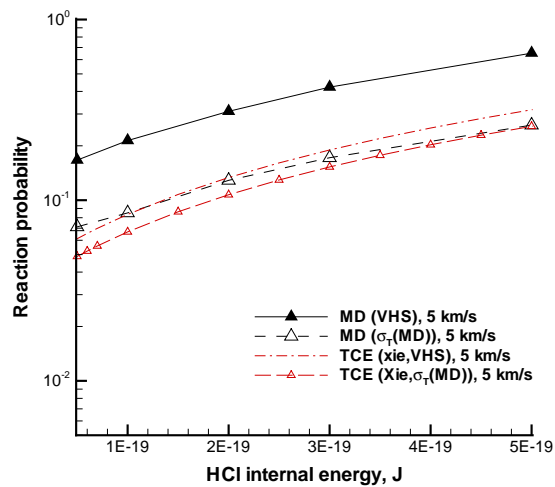


Figure 13. Comparison of the reaction probability calculated by using the reaction cross section divided by either the VHS model (Bird) or the MD/QCT total collision cross section ($\sigma_T(\text{MD})$): Reaction probabilities as a function of the reactant internal energy at 5 km/s.

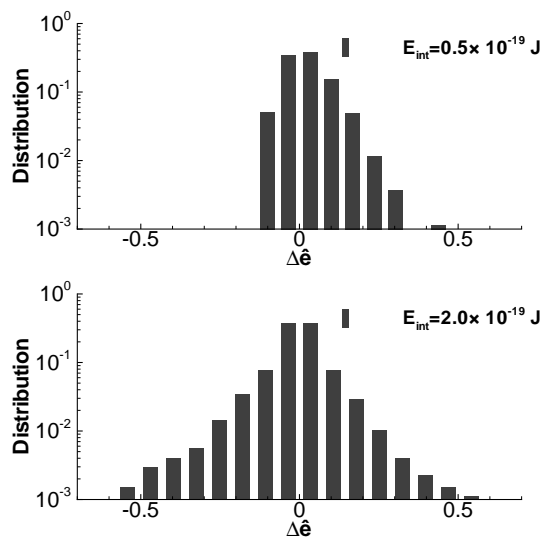


Figure 14. Distribution of the $\Delta\hat{e}_{int}$ for $E_{int} = 0.5 \times 10^{-19}$ J (top) and $E_{int} = 2.0 \times 10^{-19}$ J (bottom) at 5 km/s for O+HCl collision.

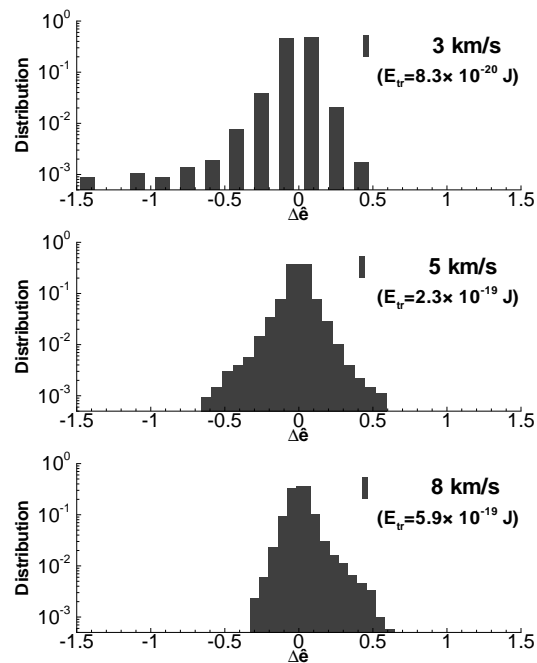


Figure 15. Distribution of the $\Delta\hat{e}_{int}$ for $E_{int} = 2.0 \times 10^{-19}$ J at 3 km/s (top), 5 km/s (middle), and 8 km/s (bottom) for O+HCl collision.

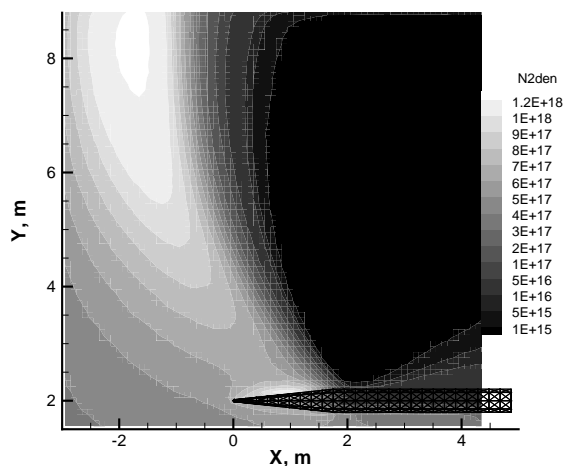


Figure 16. N_2 number density (molecule/ m^3) contours with the rate of Xie *et al* (TCE) at 120 km altitude for freestream velocity of 5 km/s. Area shown is 7.4×7.5 m.

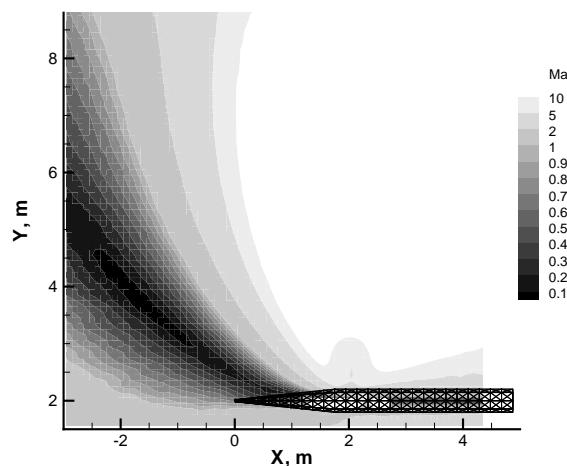


Figure 18. Mach number contours with the rate of Xie *et al* (TCE) at 120 km altitude for freestream velocity of 5 km/s. Area shown is 7.4×7.5 m.

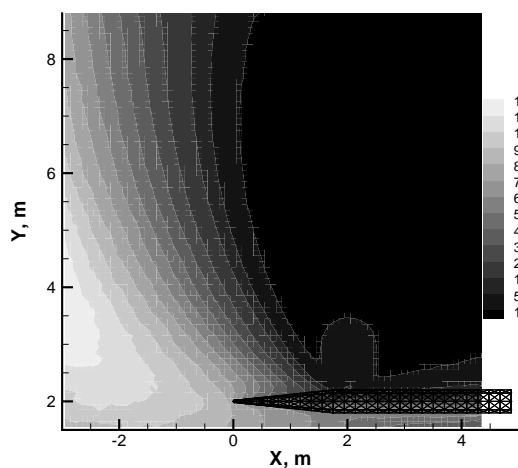


Figure 17. Translational temperature contours with the rate of Xie *et al* (TCE) at 120 km altitude for freestream velocity of 5 km/s. Area shown is 7.4×7.5 m.

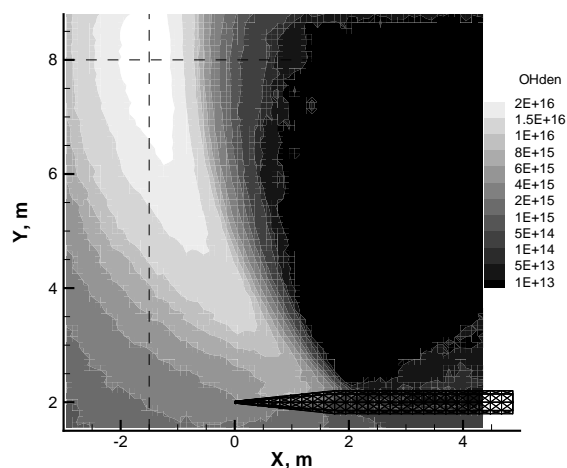


Figure 19. OH number density (molecule/ m^3) contours with the rate of Xie *et al* (TCE) at 120 km altitude for freestream velocity of 5 km/s. Area shown is 7.4×7.5 m.

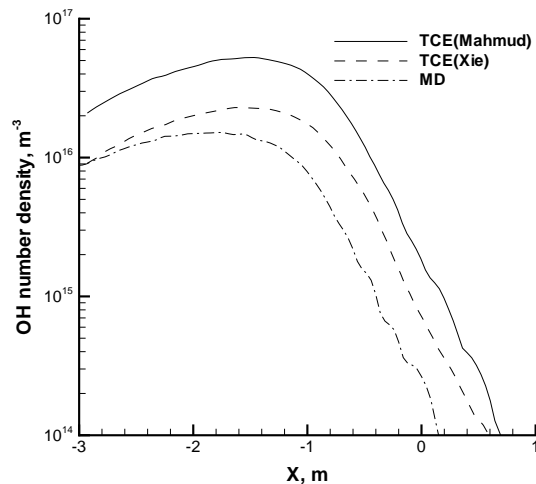


Figure 20. Comparison of OH number density (molecule/m³) at $y = 8$ m for three chemical reaction models at 120 km altitude for freestream velocity of 5 km/s.

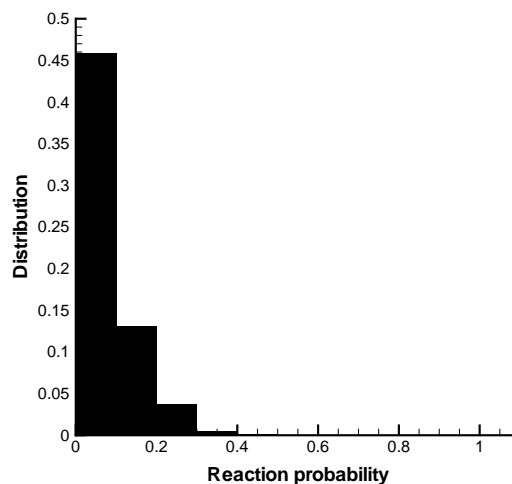


Figure 22. Reaction probability distribution for $O+HCl \rightarrow OH+Cl$ using the TCE model (the rate of Xie *et al*) for an altitude of 120 km and a freestream velocity 5 km/s.

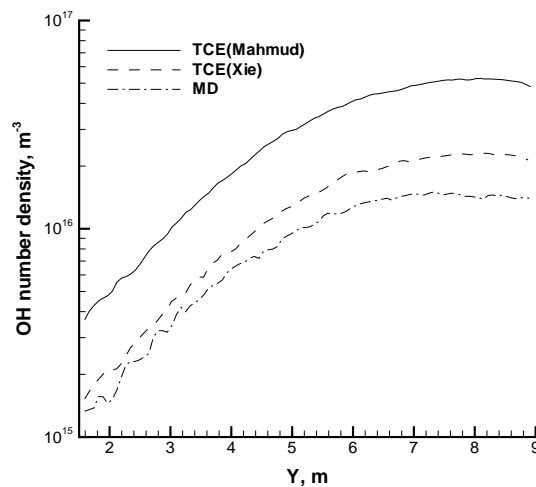


Figure 21. Comparison of OH number density (molecule/m³) at $x = -1.5$ m for three chemical reaction models at 120 km altitude for freestream velocity of 5 km/s.

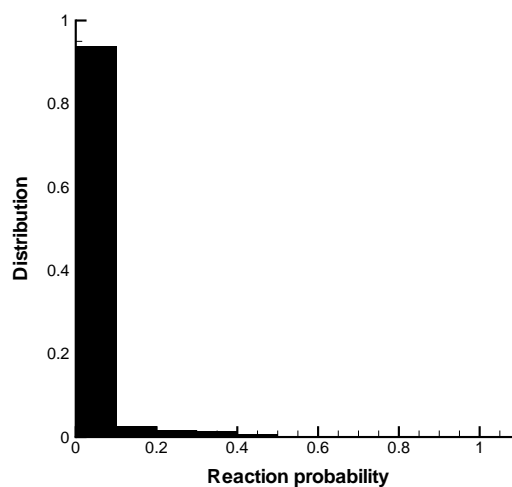


Figure 23. Reaction probability distribution for $O+HCl \rightarrow OH+Cl$ using the MD model for an altitude of 120 km and a freestream velocity 5 km/s.